THE JOURNAL OF PHYSICAL CHEMISTRY B

ARTICLE

pubs.acs.org/JPCB

Effects of High Pressure on Azobenzene and Hydrazobenzene Probed by Raman Spectroscopy

Zhaohui Dong,[†] Natashia M. Seemann,[†] Ning Lu,[†] and Yang Song*[,†]

[†]Department of Chemistry, University of Western Ontario, London, Ontario N6A 5B7, Canada

ABSTRACT: In this study, two hydrazine derivatives, azobenzene and hydrazobenzene, were compressed in a diamond anvil cell at room temperature up to 28 GPa followed by decompression. In situ Raman spectroscopy was employed to monitor the pressure-induced structural evolutions. Azobenzene was found to undergo a phase transition at ~10 GPa. Further compression to 18 GPa resulted in an irreversible breakdown of the molecular structure. Although hydrazobenzene exhibited a structural transition at a similar pressure of 10 GPa, it was found to sustain a compression pressure as high as 28 GPa without chemical reactions. The transition sequence of hydrazobenzene upon compression and decompression was thus entirely reversible in the pressure region studied, in strong contrast to that of azobenzene. The high-pressure structures of these two molecules were examined based on the spectroscopic data, and their drastically different high-pressure behaviors were analyzed and interpreted with the aid of *ab initio* molecular orbital calculations.

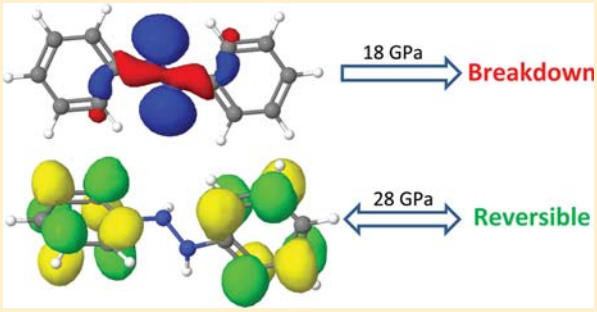

INTRODUCTION

Molecular solids are soft materials that are subject to conformational change, phase transitions, or chemical transformations upon the application of external pressures.[1−3] Compression can effectively shorten the intermolecular and intramolecular distances, thus subsequently causing reversible or irreversible modifications in the molecular structures and associated electronic, optical, or mechanical properties.[4] Therefore, pressure provides an excellent tool to produce new materials even starting from simple molecular solids, especially those with unsaturated bonds or conjugate ring structures.[5] For example, pressure-induced transformations have been reported for butadiene, benzene, furan, thiophene, pyridine, and other aromatic derivatives.[6−12] As the most basic aromatic system, in particular, benzene was found to undergo a series of pressure-induced phase transitions up to 30 GPa, beyond which pressure-induced structural amorphization was observed.[9−12] More recently, pyridine was reported to undergo a similar pressure-induced transformation sequence as benzene in a similar pressure region.[6] These pressure-induced products are interesting from a technological point of view because of their unique properties desirable for possible applications in optics, electronics, mechanics and even as coating materials for biomedical applications.[11] So far, unsaturated hydrocarbons represent a major class of materials of interest for which different reactivities of the π bonds under compressions critically influence the reaction pathways and, thus, the products.[13−15]

Azobenzene (AB) is a conjugate aromatic molecule with two phenyl rings attached to an azo group (Figure 1a). Due to its unique photochromic properties, azobenzene has been used as a moiety embedded in organic or biological macromolecules such as proteins and nucleic acids to provide special photofunctionality.[16] Moreover, based on its reversible trans−cis coupled photochemical and electrochemical isomerization,[17−19] azobenzene has been extensively studied as a photoswitch in numerous molecular systems and functional materials for applications such as high-density information storage.[20] Because the energy difference between the trans and the cis conformers is relatively small (i.e., 15 kcal·mol^{-1} or 0.6 eV), a visible photon can easily induce an electronic excitation via either the n$\rightarrow\pi^*$ or the $\pi\rightarrow\pi^*$ pathways, a topic under intense experimental and theoretical investigations.[17,18,21,22] The strong activity associated with π electrons makes azobenzene an interesting system for the examination of the combined pressure-photon effects based on the fact that both pressure and photon can effectively induce electronic excitations and thus subsequent structural transitions.[5]

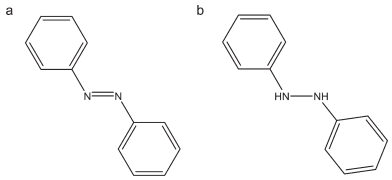

Figure 1. The molecular structures of trans-azobenzene (a) and hydrazobenzene (b).

Received: July 27, 2011
Revised: November 7, 2011
Published: November 22, 2011

In parallel, high-pressure effects on phenyl rings have been studied in a wide variety of aromatic systems in a broad pressure range. Since the N═N bond constitutes the conjugation center of azobenzene, it is expected to play a vital role responsible for the entire property of azobenzene regardless of the bulky phenyl substituents. To examine the importance of the total conjugation to the properties of azobenzene, a high-pressure study of another similar molecule, hydrazobenzene (HAB) (Figure 1b) with a broken conjugation along the N−N bond, may help to understand the isolated pressure effect on the phenyl rings and the nitrogen−nitrogen bond.

Here we report a comparative study of azobenzene and hydrazobenzene under high pressures of up to ∼28 GPa by in situ Raman spectroscopy. Our results suggest strongly contrasting high-pressure behaviors between these two compounds. Moreover, a study of the high-pressure effect on N═N and N−N bonds may provide valuable insight into the development of high energy density materials that contain singly bonded nitrogens.[23]

EXPERIMENTAL SECTION

Both azobenzene (96%) and hydrazobenzene (99%) were purchased from Aldrich and were used without further purification. Azobenene appears as orange crystals, whereas hydrazobenzene is mostly colorless and transparent. A symmetric diamond anvil cell with a pair of type Ia diamonds with a 400-μm culet was used. A hole with a diameter of 150 μm was drilled in a stainless steel gasket as the sample chamber. A few ruby chips were inserted in the sample chamber as the pressure calibrant using the well-established R_1 ruby fluorescence band shift.[24] The accuracy of the pressure measurement was estimated to be ±0.05 GPa under quasi-hydrostatic conditions.[25] No pressure transmitting medium was used for either sample.

In situ high-pressure Raman measurements were carried out using a customized Raman microspectroscopy system. A He−Ne laser with a wavelength of 632.8 nm was used as the excitation source. The Raman system was equipped with an Olympus microscope, which can focus the laser to less than a 5 μm diameter on the sample. The laser power measured on the sample was less than 5 mW. The Raman system adopted a backscattering geometry, and the scattered light was dispersed using an imaging spectrograph equipped with a 1200 lines/mm grating, achieving a resolution of 0.2 cm^{-1}. The system was calibrated using neon lines with an uncertainty of ±1 cm^{-1}. An edge filter was installed to remove the Rayleigh and anti-Stokes lines enabling a measurable spectral range above ∼100 cm^{-1}. The Raman signal was then recorded using an ultrasensitive liquid-nitrogen-cooled, back-illuminated CCD detector from Acton. The Raman spectra were collected in several spectral windows to cover the entire region of interest (i.e., 100−3500 cm^{-1}) and to avoid the interference from the dominant diamond Raman band at ∼1340 cm^{-1}. During data acquisition, all parameters (e.g., laser power, accumulation time, etc.) were kept the same, such that the Raman intensities from different spectra were qualitatively comparable and, thus, were normalizable. All Raman measurements were conducted at room temperature and were reproduced several times.

RESULTS AND DISCUSSION

A. Raman Spectra of AB and HAB at Ambient Pressure. The Raman spectra of both azobenzene and hydrazobenzene at ambient condition are shown in Figure 2. Azobenzene adopts the trans-configuration as the more thermally stable form with the two phenyl rings on opposite sides of the N═N bond thus exhibiting a C_{2h} symmetry (Figure 1a). Therefore, a total of 66 normal vibrational modes, out of which 33 are Raman active (10 B_g, out-of-plane and 23 A_g, in-plane modes), are expected for a single azobenzene molecule.[26,27] Solid azobenzene is known to have a monoclinic crystal structure with a space group $P2_1/a$ and $Z = 2$,[21] and thus 66 Raman active modes are predicted. In our Raman measurements, however, only 18 modes were observed indicating that the magnitude of the correlation field splitting was small and cannot be observed with the current experimental set up. The assignment of each Raman mode is listed in Table 1 in comparison with previous studies of azobenzene in the trans-configuration. As can be seen, our Raman measurements agree with those obtained in both the theoretical and experimental studies.[18,26,28,29] Hydrazobenzene does not exhibit a significant molecular symmetry due to the free rotation along the N−N bond and thus all vibrational modes are Raman active. However, due to the very similar molecular skeleton to azobenzene, hydrazobenzene has a very similar Raman spectrum correspondingly, except that most Raman modes of hydrazobenzene shift to lower frequencies due to the replacement of the N═N bond by the N−N single bond. The Raman peaks for hydrazobenzene in this study are therefore assigned by adopting the assignment for azobenzene without rigor (with the corresponding Raman modes labeled by a prime), due to the lack of assignment from previous studies. In the Raman spectrum for hydrazobenzene, the bands at 3329 cm^{-1} and 1027 cm^{-1} are assigned as the N−H and N−N stretching vibrational modes, respectively, while the band observed at 845 cm^{-1} is assigned as the H−N−N−H bending mode.

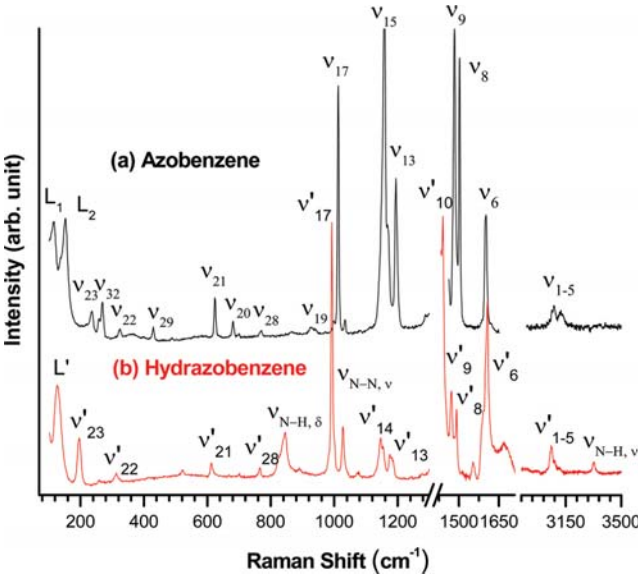

Figure 2. Raman spectra of azobenzene (a) and hydrazobenzene (b) collected at ambient conditions. The two spectra are offset vertically for clarity. The spectral region of 1250−1400 cm^{-1} is omitted due to the strong T_{2g} Raman mode of the diamond anvils.

B. Raman Spectra of AB on Compression and Decompression. Selected Raman spectra of azobenzene collected upon compression at pressures of up to 17.8 GPa followed by decompression are shown in Figure 3. As the pressure increased,

Table 1. Assignment and Frequencies (cm^{-1}) of Observed Raman Internal Modes of Azobenzene (AB) and Hydrazobenzene (HAB) in Comparison with References

		reference		this work	
Raman mode[a]	assignment[b]	calculation[c]	experimental[d]	AB	HAB
ν_{N-H}	N−H stretching				3329
ν_1 (A_g)	phenyl C−H stretching	3221	*3085*	3074	3058
ν_2 (A_g)	phenyl C−H stretching	3210	*3073*		
ν_3 (A_g)	phenyl C−H stretching	3197	*3066*		
ν_4 (A_g)	phenyl C−H stretching	3187	*3060*		
ν_5 (A_g)	phenyl C−H stretching	3178	*3044*		
ν_6 (A_g)	phenyl C−C stretching	1622	1591/*1595*	1601	1607
ν_7 (A_g)	phenyl C−C stretching	1614			
ν_8 (A_g)	azo stretching	1519	1491/*1443*	1502	1491
ν_9 (A_g)	azo stretching	1504	1470/*1493*	1480	1471
ν_{10} (A_g)	azo stretching	1450	1440/*1473*		1440
ν_{11} (A_g)	phenyl C−H bending	1395	1312/*1379*		
ν_{12} (A_g)	phenyl C−H bending	1368	*1315*		
ν_{13} (A_g)	phenyl C−H bending	1235	1185/*1184*	1194	1176
ν_{14} (A_g)	phenyl C−H bending	1226	1155/*1158*	1168	1147
ν_{15} (A_g)	C−N bending	1195	1143/*1146*	1157	
ν_{16} (A_g)	phenyl C−C stretching	1110	1068/*1071*	1033	
ν_{N-N}	N−N stretching				1027
ν_{17} (A_g)	phenyl C−H bending	1047	1021/*1023*	1013	992
ν_{18} (A_g)	phenyl C−H bending	1024	1000/*1003*	998	
ν_{19} (A_g)	C−N bending	933	914/*913*	931	
ν_{N-H}	H−N−N−H bending				845
ν_{20} (A_g)	C−N bending	691	*667*/*670*	682	
ν_{21} (A_g)	phenyl C−H bending	634	*611*/*614*	623	613
ν_{22} (A_g)	C−N bending	307		324	313
ν_{23} (A_g)	C−N bending	226	*219*	235	196
ν_{24} (B_g)	phenyl C−H wagging	857	*968*		
ν_{25} (B_g)	phenyl C−H wagging	851	*967*/*938*		
ν_{26} (B_g)	phenyl C−H wagging	825	935		
ν_{27} (B_g)	phenyl C−H wagging	778	834/*836*		
ν_{28} (B_g)	phenyl C−H wagging	702	*773*/*755*	770	765
ν_{29} (B_g)	phenyl C−H wagging	444		430	
ν_{30} (B_g)	phenyl C−H wagging	400			
ν_{31} (B_g)	phenyl C−H wagging	381	*406*/*403*		
ν_{32} (B_g)	phenyl flags	213	*218*/*251*	269	
ν_{33} (B_g)	phenyl flags	−85			

[a] The symmetry in the parentheses refers to azobenzene only, while the mode numbering applies to both compounds (i.e., with the prime omitted for hydrazobenzene). [b] References 26. and 27. [c] Reference 26. [d] Frequencies in regular font are from ref 28, while those in italics are from ref 29.

all the Raman bands shifted progressively toward higher frequencies accompanied by peak broadening. Other than the blue shift, all the internal modes (>200 cm^{-1}) maintained the ambient-pressure Raman profile until 10.4 GPa, indicating that the azobenzene molecular structure was stable below 10.4 GPa. Compression beyond 10.4 GPa resulted in the dramatically reduced intensity of all the internal modes with the Raman modes below 1000 cm^{-1} being significantly depleted. Concurrently, two new bands at 565 cm^{-1} and 733 cm^{-1} became prominent at pressures above 10.4 GPa (Figure 3). These two bands appeared to be even more intense with increasing the pressure up to 16.0 GPa. In addition, the triple peaks initially located at 1160 cm^{-1} eventually merged to a single broad peak at this pressure. Finally, all Raman peaks vanished at the highest pressure achieved in this study for azobenzene (i.e., 17.8 GPa). The featureless Raman profile at high pressures suggested that azobenzene had undergone a major structural modification.

Consistent with the high-pressure behavior of internal vibrational modes, the external modes (<200 cm^{-1}) also shifted to a higher frequency upon compression but were more prominently accompanied with major changes of the lattice profile. For instance, a new lattice mode at 148 cm^{-1} was observed at 3.6 GPa. All the lattice modes sustained up to 10.4 GPa and completely vanished beyond this pressure (Figure 3). The disappearance of external Raman modes strongly suggests a structural amorphization at pressure of 10.4 GPa, whereas the complete

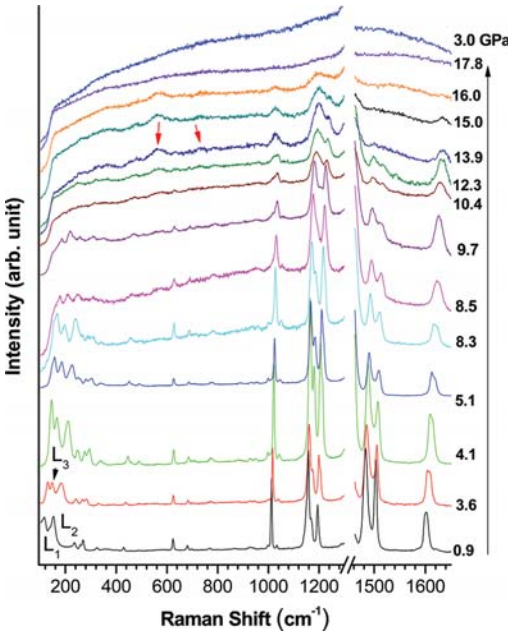

Figure 3. Selected Raman spectra of azobenzene collected along a compression−decompression cycle at room temperature in the region of 100−1700 cm^{-1}. The relative intensities are normalized and thus are directly comparable. The pressures in gigapascals are labeled for each spectrum. The vertical long arrow on the right shows the sequence of the compression. Two red arrows indicate new peaks appearing at high pressures. The spectra are offset vertically for clarity.

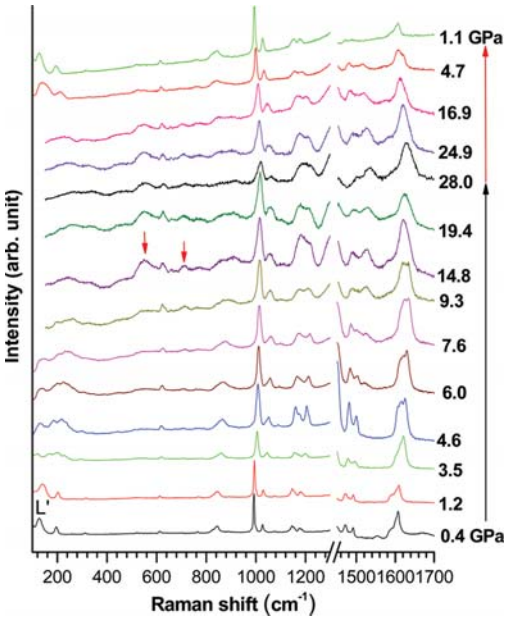

Figure 4. Selected Raman spectra of hydrazobenzene collected along a compression−decompression cycle at room temperature in the region of 100−1700 cm^{-1}. The relative intensities are normalized and thus are directly comparable. The pressures in gigapascals are labeled for each spectrum. The long arrows represent compression and decompression sequence in black and red, respectively. Two short arrows (red) show new peaks appeared at high pressures. The spectra are offset vertically for clarity.

destruction of all Raman modes at 17.8 GPa can be attributed to a chemical transformation. Upon releasing the pressure, no Raman mode was recovered indicating that the pressure-induced transformation at 17.8 GPa was completely irreversible.

C. Raman Spectra of HAB on Compression and Decompression. Selected Raman spectra of hydrazobenzene on compression and decompression are shown in Figure 4. Upon compression, the internal modes shifted to a higher frequency accompanied with peak broadening, similar to those observed in azobenzene. However, the Raman spectrum did not change significantly with pressures of up to 9.3 GPa. The most noticeable change was that two lattice modes at 168 cm^{-1} and 229 cm^{-1}, which were first observed at 3.5 GPa and then vanished at 9.3 GPa, suggesting the possible distortion of the molecular crystal lattice. Above 9.3 GPa, some internal modes below 1000 cm^{-1} disappeared. This observation further indicates the pressure-induced structural disorder and the eventual amorphization upon compression above this pressure. Concurrently, two new bands at 551 cm^{-1} and 712 cm^{-1} were observed above this pressure, which were also found in azobenzene upon compression, indicating the enhanced intermolecular interactions due to the smaller intermolecular distances. However, the most dominant Raman modes of hydrazobenzene could still be observed easily (e.g., at 1020 cm^{-1}) at the highest pressure achieved in this study (i.e., 27.8 GPa), in strong contrast to azobenzene.

Upon decompression, most Raman modes of the hydrazobenzene followed a similar backward pressure sequence as upon compression. In particular, the two new bands observed above 9.3 GPa on compression as transient bands disappeared at 4.7 GPa during decompression. When pressure was released to ambient, we were able to recover the Raman spectrum of

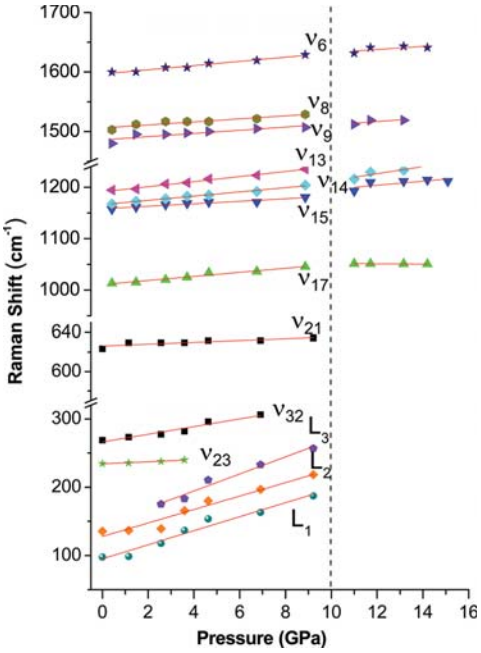

Figure 5. Pressure dependence of the Raman modes of azobenzene on compression. Solid straight lines are linear fits to the data. The vertical dashed line denotes the suggested transition boundary. Different symbols denote different Raman modes with assignment labeled.

hydrazobenzene that was almost identical to that observed before compression in the entire spectral region, indicating that the

phase transformation observed in hydrazobenzene was totally reversible.

D. Pressure Effects on Raman Modes of AB and HAB. Pressure dependences of selected Raman modes of azobenzene and hydrazobenzene on compression are depicted in Figures 5 and 6, respectively. Since the C−H stretching modes of azobenzene at 2800−3200 cm^{-1} were clearly observed only below 3.5 GPa, they are not included in the analysis here. The pressure dependences ($d\nu/dP$) of the selected Raman modes are listed in Table 2 as well. In general, all Raman modes exhibited pressure-induced blue shifts except the N−H stretching bond of hydrazobenzene as discussed below, consistent with that the bonds become stiffened by pressure. However, in different pressure regions, the shift rates are different, providing evidence for phase transformations.

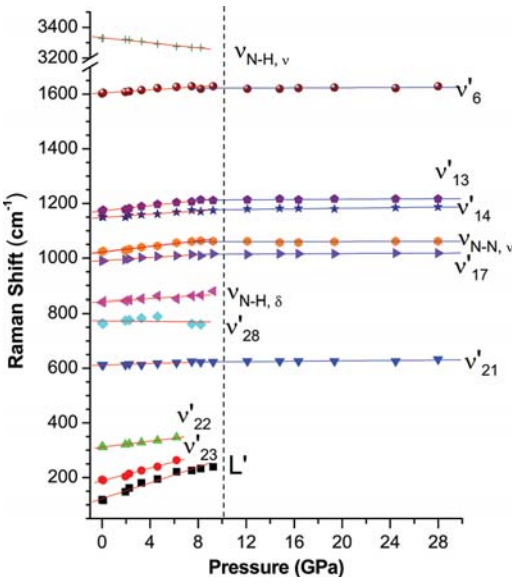

Figure 6. Pressure dependence of the Raman modes of hydrazobenzene on compression. Solid straight lines are linear fits to the data. The vertical dashed line marks the suggested phase transition boundary. Different symbols denote different Raman modes with assignment labeled besides.

A possible solid to solid phase transition occurs at about 10.0 GPa in azobenzene as indicated by the vertical dashed line in Figure 5. Below this pressure, Raman modes in the low frequency region, such as the phenyl flag mode (ν_{32}) and the lattice modes (L_1, L_2, and L_3), are more sensitive to pressure suggested by the relatively larger pressure coefficients ($d\nu/dP$), in contrast to the internal Raman modes in the higher frequency region (>600 cm^{-1}) as summarized in Table 2. Similarly, the vertical dashed line in Figure 6 denotes the phase transition boundary in hydrazobenzene at about 10.0 GPa. The lattice mode (L′ at 121 cm^{-1}) and the C−N bending mode (ν'_{23} at 196 cm^{-1}) are highly sensitive to compression with the largest pressure coefficients of 14.5 cm^{-1}/GPa and 11.6 cm^{-1}/GPa, respectively. Moreover, most Raman modes show a positive slope below 10 GPa except the N−H stretching mode at 3329 cm^{-1}, which has a strongly negative slope (i.e., −8.3 cm^{-1}/GPa). The mode softening in this case can be interpreted as the N−H bond weakening as a result of the formations of hydrogen bonding with neighboring N−H bonds during the compression. In addition, most Raman modes had generally larger slopes (i.e., > 2 cm^{-1}/GPa) before the phase transformation than those after (i.e., < 0.5 cm^{-1}/GPa), indicating a smaller compressibility for HAB in the higher pressure region as a result of denser molecular packing upon compression.

E. Discussion. Although both azobenzene and hydrazobenzene underwent a pressure-induced structural transformation at the same pressure of around 10.0 GPa, the nature of the transformation was drastically different. In particular, the transition of azobenzene was initiated by structural disorder at 10.0 GPa followed by complete amorphization above 17.8 GPa as evidenced by the disappearance of all the characteristic Raman modes. The irreversible amorphization suggests that the transformation was chemical in nature, possibly via a polymerization process, resulting in highly disordered cross-linked structures. Such a chemical transformation was accompanied by the striking change in the physical appearance of the sample: the original transparent orange crystals turned completely gray and sooty upon compression, and the gray sample showed no change after the pressure was completely released. Pressure-induced

Table 2. Pressure Dependence $d\nu/dP$ (cm^{-1}/GPa) of Raman Modes of Azobenzene and Hydrazobenzene

azobenzene				hydrazobenzene			
Raman mode	frequency (cm^{-1})	0−10 GPa	10−16 GPa	Raman mode[b]	frequency (cm^{-1})	0−10 GPa	10−28 GPa
ν_6	1590	3.1	2.4	$\nu_{N-H,\ \nu}$	3329	- 8.3	
ν_8	1483	2.2		ν'_6	1607	2.8	0.1
ν_9	1460	2.3	2.6	ν'_{13}	1176	4.8	0.2
ν_{13}	1182	4.5		ν'_{14}	1147	3.0	0.5
ν_{14}	1156	4.9	6.3	$\nu_{N-N,\ \nu}$	1027	5.1	0.1
ν_{15}	1142	3.7	3.6	ν'_{17}	992	2.8	0.2
ν_{17}	998	2.8	- 0.2	$\nu_{N-H,\ \delta}$	845	2.7	
ν_{21}	605	0.8		ν'_{28}	765	- 0.4	
ν_{32}	243	5.6		ν'_{21}	613	1.4	0.4
ν_{23}	235	4.8		ν'_{22}	313	5.4	
L_3	183[a]	12.5		ν'_{23}	196	11.6	
L_2	135	9.8		L′	121	14.5	
L_1	98	10.3					

[a] Observed at 3.6 GPa. [b] Subscript ν: stretching; δ: bending.

dx.doi.org/10.1021/jp207170w |J. Phys. Chem. B 2011, 115, 14912–14918

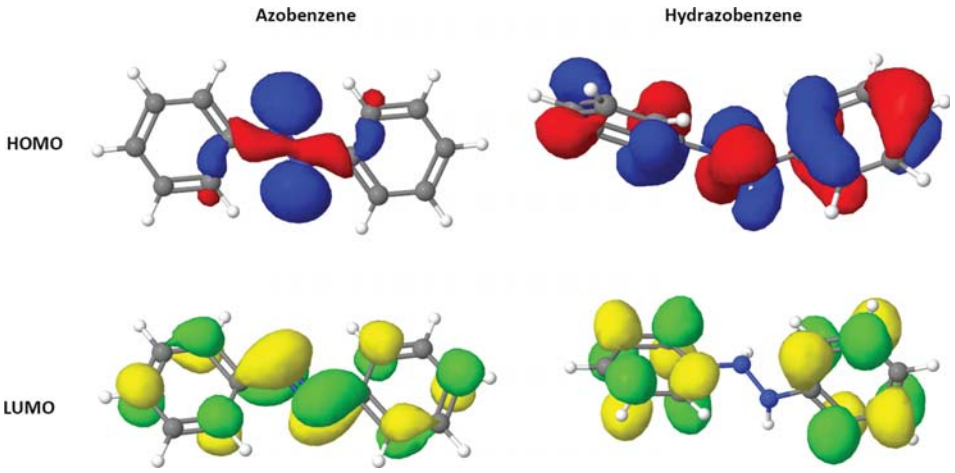

Figure 7. The frontier orbitals, i.e., HOMO (top row) and LUMO (bottom row) orbitals of azobenzene (left column) and hydrazobenzene (right column) calculated at the B3LYP/6-311+G(d,p) level of theory. An arbitrary isosurface value was used for all the plots.

amorphization has also been reported in other organic molecular crystals such as benzophenone[30] at 11 GPa and hexanmethylenetetramine[31] at 15 GPa. In addition, interesting transformations that are believed to involve the formation of a polymerized phase were also observed in acetophenone azine, which has a similar structure as azobenzene.[32] From the high-pressure Raman spectra, we suggest that the polymerization occurs involving the entire molecule instead of the preferential transformation of the N═N double bond to the N−N single bond. This was evidenced by the absence of the N−N characteristic vibrational frequency at 1023 cm^{-1}, which would have been observed if the N═N double bond were to be converted to a N−N single bond, and the fact that the azo stretching modes (e.g., ν_8 and ν_9) responded to compression concertedly with those of the phenyl ring vibrations (e.g., ν_6 and ν_{16}) in the polymerization process.

More detailed polymerization mechanisms can be understood in parallel with benzene, the basic building unit of azobenzene. Similarly, benzene was reported to polymerize or amorphize by compression but at a much higher pressure (i.e., > 30 GPa) by Ciabini et al.[11,12] Their studies suggest that when a threshold distance (2.6 Å) between two carbon atoms on adjacent benzene rings is reached by compression, the polymerization process can be triggered by fluctuations in the atom positions that are caused by thermal vibrations. Theoretical calculations of the process indicate large fluctuations on a femtosecond time scale occurring in the electron density distribution between newly bonded atom pairs.[11] These extremely fast charge fluctuations propagated throughout the compressed benzene lattice and resulted in the formation of an amorphous network of linked carbon rings. Considering azobenzene as an extended aromatic system of benzene rings, the polymerization may occur in a similar manner, except that the threshold pressure is much lower for bulkier monomers.

In contrast, hydrazobenzene is much more stable under high pressure. The reversible phase transition is physical rather than chemical, i.e., it is characterized by the distortion rather than the destruction of the skeleton of molecules under high pressure. Instead of having a planar configuration reinforced by the N═N double bond in azobenzene, hydrazobenzene contains only a N−N single bond, which allows the free rotation of the two phenyl rings along the N−N axis. Thus, the net pressure effect on hydrazobenzene can be understood as being the modification of the molecular conformation that takes place before a polymeric reaction involving the phenyl ring occurs. This pressure-induced conformational change accompanied with structural disordering has been observed in other smaller molecular crystals.[1]

From the above comparisons, it is therefore easy to understand why the two hydrazine derivatives behave so differently under high pressure. It is the complete conjugate electronic configuration of azobenzene that makes the entire molecule subject to cross-linking, whereas hydrazobenzene behaves almost equivalently like independent benzene rings. We therefore speculate that upon compression to a higher pressure (e.g., > 30 GPa), similar irreversible transformations may be observed as those for benzene. To confirm the different reactivities of azobenzene and hydrazobenzene, we performed *ab initio* molecular orbital calculations based on the DFT method using the GASSIAN 98 program package.[33] Previous extensive DFT calculations using the gradient corrected hybrid B3LYP functional have reproduced the geometries and the vibrational properties of azobenzene reasonably well.[18,22,34] It was also demonstrated that the incorporation of diffuse functions and polarization functions could improve the estimation of various properties of azobenzene. Therefore, in our calculations we chose the prevailing B3LYP functional with Pople's basis set 6-311+G(d, p), which is comparable or slightly better than that of previous studies.[18,22] Figure 7 shows the frontier orbitals that would contribute to the polymerization process if the irreversible chemical transformation occurs. We note that Crecca and Roitberg[22] reported very similar frontier molecular orbitals for azobenzene using density functional theories at a similar level of theory, i.e., B3LYP/6-31G* (Figure 3 of ref 22), but no corresponding studies had been performed on hydrazobenzene before. As can be seen, the LUMO orbital of azobenzene shows a reinforced conjugation with the contribution of the π ($2p_z$ of carbon and nitrogen) orbitals especially by nitrogen atoms, whereas the electron density for hydrazobenzene is mainly situated on the phenyl carbons rather than the two nitrogens, consistent with the above interpretation. In addition, our calculation shows a HOMO−LUMO gap of 3.91 eV for azobenzene, also in good agreement with that calculated by Crecca and Roitberg.[22] Compared to the gap of 5.19 eV for hydrazobenzene, the 25% smaller energy gap for azobenzene may correlate with its higher reactivity upon compression. Such a level of calculations, therefore, provides a reasonably good,

qualitative understanding of the different pressure behaviors of the two hydrazine derivatives.

CONCLUSIONS

Using in situ Raman spectroscopy, we investigated the structures and transformations of azobenzene and hydrazobenzene at high pressures of up to 28 GPa, comparatively. Upon compression, both compounds exhibited a pressure-induced structural transition at around 10 GPa. Further compression of azobenzene to 18 GPa resulted in an irreversible destruction of the molecular structure. In contrast, hydrazobenzene was found to sustain pressures up to 28 GPa without chemical transformations, and the structural evolutions with pressure were totally reversible in the entire pressure region. The high-pressure behaviors and possible structures of these two molecules were analyzed in comparison with the results of previous studies on other aromatic structures. While hydrazobenzene retains a disordered but chemically stable phase at high pressures, azobenzene undergoes an amorphization process accompanied by polymerization via cross-linking involving the entire molecule. The drastically different high-pressure stabilities of the two compounds are attributed to their intrinsically different electronic configurations in terms of conjugation. The molecular orbital calculations using density functional theories further supported the experimental observations and the spectroscopic interpretations.

AUTHOR INFORMATION

Corresponding Author

*Phone: (519)661-2111 ext. 86310. Fax: (519)661-3022. E-mail: yang.song@uwo.ca.

ACKNOWLEDGMENT

The authors are grateful to M. J. Walzak at Surface Science Western for her partial technical assistance. The authors also acknowledge the support from a Discovery Grant and a Research Tools and Instruments Grant from the Natural Sciences and Engineering Council of Canada, a Leading Opportunity Fund from the Canadian Foundation for Innovation, and an Early Researcher Award from the Ontario Ministry of Research and Innovation.

REFERENCES

(1) Sabharwal, R. J.; Huang, Y. N.; Song, Y. *J. Phys. Chem. B* **2007**, *111*, 7267–7273.
(2) Dong, Z.; Beilby, N. G.; Huang, Y.; Song, Y. *J. Chem. Phys.* **2008**, *128* (074501), 1–9.
(3) Murli, C.; Song, Y. *J. Phys. Chem. B* **2010**, *114*, 9744–9750.
(4) Hemley, R. J. *Annu. Rev. Phys. Chem.* **2000**, *51*, 763–800.
(5) Bini, R. *Acc. Chem. Res.* **2004**, *37*, 95–101.
(6) Zhuravlev, K. K.; Traikov, K.; Dong, Z. H.; Xie, S. T.; Song, Y.; Liu, Z. X. *Phys. Rev. B* **2010**, *82* (064116), 1–8.
(7) Citroni, M.; Ceppatelli, M.; Bini, R.; Schettino, V. *J. Chem. Phys.* **2003**, *118*, 1815–1820.
(8) Citroni, M.; Ceppatelli, M.; Bini, R.; Schettino, V. *Chem. Phys. Lett.* **2003**, *367*, 186–192.
(9) Pruzan, P.; Chervin, J. C.; Thiery, M. M.; Itie, J. P.; Besson, J. M.; Forgerit, J. P.; Revault, M. *J. Chem. Phys.* **1990**, *92*, 6910–6915.
(10) Ciabini, L.; Santoro, M.; Bini, R.; Schettino, V. *Phys. Rev. Lett.* **2002**, *88* (085505), 1–4.
(11) Ciabini, L.; Santoro, M.; Gorelli, F. A.; Bini, R.; Schettino, V.; Raugei, S. *Nat. Mater.* **2007**, *6*, 39–43.
(12) Ciabini, L.; Santoro, M.; Bini, R.; Schettino, V. *J. Chem. Phys.* **2002**, *116*, 2928–2935.
(13) Chelazzi, D.; Ceppatelli, M.; Santoro, M.; Bini, R.; Schettino, V. *J. Phys. Chem. B* **2005**, *109*, 21658–21663.
(14) Schettino, V.; Bini, R. *Chem. Soc. Rev.* **2007**, *36*, 869–880.
(15) Ceppatelli, M.; Fontana, L. *Phase Transitions* **2007**, *80*, 1085–1101.
(16) Asanuma, H.; Ito, T.; Yoshida, T.; Liang, X. G.; Komiyama, M. *Angew. Chem., Int. Ed.* **1999**, *38*, 2393–2395.
(17) Tanaka, S.; Itoh, S.; Kurita, N. *Chem. Phys. Lett.* **2002**, *362*, 467–475.
(18) Stepanic, V.; Baranovic, G.; Smrecki, V. *J. Mol. Struct.* **2001**, *569*, 89–109.
(19) Tong, X.; Pelletier, M.; Lasia, A.; Zhao, Y. *Angew. Chem. Int. Ed.* **2008**, *47*, 3596–3599.
(20) Liu, Z. F.; Hashimoto, K.; Fujishima, A. *Nature* **1990**, *347*, 658–660.
(21) Harada, J.; Ogawa, K. *J. Am. Chem. Soc.* **2004**, *126*, 3539–3544.
(22) Crecca, C. R.; Roitberg, A. E. *J. Phys. Chem. A* **2006**, *110*, 8188–8203.
(23) Eremets, M. I.; Gavriliuk, A. G.; Trojan, I. A.; Dzivenko, D. A.; Boehler, R. *Nat. Mater.* **2004**, *3*, 558–563.
(24) Mao, H. K.; Bell, P. M.; Shaner, J. W.; Steinberg, D. J. *J. Appl. Phys.* **1978**, *49*, 3276–3283.
(25) Mao, H. K.; Xu, J.; Bell, P. M. *J. Geophys. Res., [Solid Earth Planets]* **1986**, *91*, 4673–4676.
(26) Armstrong, D. R.; Clarkson, J.; Smith, W. E. *J. Phys. Chem.* **1995**, *99*, 17825–17831.
(27) Tecklenburg, M. M. J.; Kosnak, D. J.; Bhatnagar, A.; Mohanty, D. K. *J. Raman Spectrosc.* **1997**, *28*, 755–763.
(28) Gruger, A.; Lecalve, N. *J. Chim. Phys. Phys.-Chim. Biol.* **1972**, *69*, 743.
(29) Kellerer, B.; Brandmul., J; Hacker, H. H. *Indian J. Pure Appl. Phys.* **1971**, *9*, 903.
(30) Zhang, D. L.; Lan, G. X.; Hu, S. F.; Wang, H. F.; Zheng, J. M. *J. Phys. Chem. Solids* **1995**, *56*, 27–33.
(31) Rao, R.; Sakuntala, T.; Deb, S. K.; Roy, A. P.; Vijayakumar, V.; Godwal, B. K.; Sikka, S. K. *Chem. Phys. Lett.* **1999**, *313*, 749–754.
(32) Tang, X. D.; Ding, Z. J.; Zhang, Z. M. *Solid State Commun.* **2009**, *149*, 301–306.
(33) Frisch, M. J. T., G. W.; Schlegel, H. B.; Scuseria, G. E.; Robb, M. A.; Cheeseman, J. R.; Zakrzewski, V. G.; Montgomery, J. A., Jr.; Stratmann, R. E.; Burant, J. C.; Dapprich, S.; Millam, J. M.; Daniels, A. D.; Kudin, K. N.; Strain, M. C.; Farkas, O.; Tomasi, J.; Barone, V.; Cossi, M.; Cammi, R.; Mennucci, B.; Pomelli, C.; Adamo, C.; Clifford, S.; Ochterski, J.; Petersson, G. A.; Ayala, P. Y.; Cui, Q.; Morokuma, K.; Salvador, P.; Dannenberg, J. J.; Malick, D. K.; Rabuck, A. D.; Raghavachari, K.; Foresman, J. B.; Cioslowski, J.; Ortiz, J. V.; Baboul, A. G.; Stefanov, B. B.; Liu, G.; Liashenko, A.; Piskorz, P.; Komaromi, I.; Gomperts, R.; Martin, R. L.; Fox, D. J.; Keith, T.; Al-Laham, M. A.; Peng, C. Y.; Nanayakkara, A.; Challacombe, M.; Gill, P. M. W.; ohnson, B. ;Chen, J. W.; Wong, M. W.; Andres, J. L.; Gonzalez, C.; Head-Gordon, M.; Replogle, E. S. Pople, J. A. Inc.: Pittsburgh, PA, 2001.
(34) Biswas, N.; Umapathy, S. *J. Phys. Chem. A* **1997**, *101*, 5555–5566.